COMPOSITIONAL DIVERSITY OF PYROCLASTICS IN J. HERSCHEL CRATER AND AROUND LAVOISIER CRATER. J. D. Stopar[1], H. Vannier[2], L. R. Gaddis[1], K. Ivey[1], B. Horgan[2], K. Bennett[3], T. Giguere[4], [1]Lunar and Planetary Institute, USRA, Houston, TX, [2]Purdue University, West Lafayette, IN, [3]USGS Astrogeology, Flagstaff, AZ, [4]University of Hawaii, Honolulu, HI

Introduction: A low-albedo pyroclastic deposit occurs on the east side of J. Herschel crater (-37.2°E, 61.8°N) (**Fig. 1**) [1-5]. This deposit exhibits UVVIS-NIR spectral characteristics suggesting the presence of Fe-bearing glass or perhaps olivine [1-4]. Low-albedo deposits also occur in several areas in Lavoisier crater and some nearby locations (-80.0°E, 39.0°N) (**Fig. 1**). The Lavoisier deposits exhibit spectral characteristics also indicative of Fe-bearing glass [6,7]. Lunar pyroclastic deposits are thought to generally originate from deep within the Moon and may represent some of the earliest volcanic deposits as well as the least fractionated during ascent and eruption [e.g., 8] and many contain species with unresolved resource potential [9,10]. Thus, it is essential that we gain an improved understanding and characterize their compositions and origins. Here we focus on pyroclastic deposits at J. Herschel and Lavoisier craters on the northwest lunar near side to characterize: 1) the major Fe-bearing components, including pyroxene, olivine, and volcanic glass to investigate how the deposits may have formed; and 2) the morphology and possible eruption characteristics of the deposits.

Data and Methods: Calibrated data from LRO's Narrow Angle Camera (NAC), Wide Angle Camera (WAC), Kaguya/SELENE's Multiband Imager (MI), Kaguya/SELENE's Terrain Camera (TC), and Chandrayaan's Moon Mineralogy Mapper (M^3) provide new insights into the low-albedo deposits. Data were utilized to assess deposit morphology at ~0.5- to 2-m scales (NAC [11]), albedo at 100-m and 400-m scales (WAC [12]), topography at the ~10 m and ~60 m scale (TC DTM and SLDEM [13,14]), composition from nine bandpasses (MI pixel scales of ~20 m and 62 m [15,16]), and composition (446 to 3000 nm) at ~80 or 140 m scales (M^3 [17]) and multispectral 100 m maps (Clementine [18]). Spectral data were corrected for thermal effects, we removed the continuum slope, and we calculated band parameters [19-21]. The position, depth, and asymmetry of the 1- and 2-micron spectral features can be used to study olivine, clinopyroxene, orthopyroxene, plagioclase feldspar, and basaltic glass components [e.g., 1-4, 20-22].

J. Herschel: Dark mantling deposits (DMD) occur along an irregular network of fractures in the eastern floor of J. Herschel crater. The concentrations of DMDs around several irregular pits and craters suggest multiple sources along a complex fissure [1,5,24]. Four irregular craters or vents are associated with the dark deposit (**Fig. 1**). J. Herschel crater exhibits a roughly domed profile in elevation data, with the pyroclastics located along fractures at the edge.

Composition: Our analyses of spectra are consistent with those previously described [1-4]. In MI spectra, the 1-micron band decreases in strength and narrows with distance from the vent [24]. The deposits also have asymmetric 1-micron bands with centers at wavelengths >1000 nm, consistent with olivine or a mixture of low-Ca pyroxene and Fe-bearing glass [1,3,4,21,24]. TiO_2 content of the area is apparently

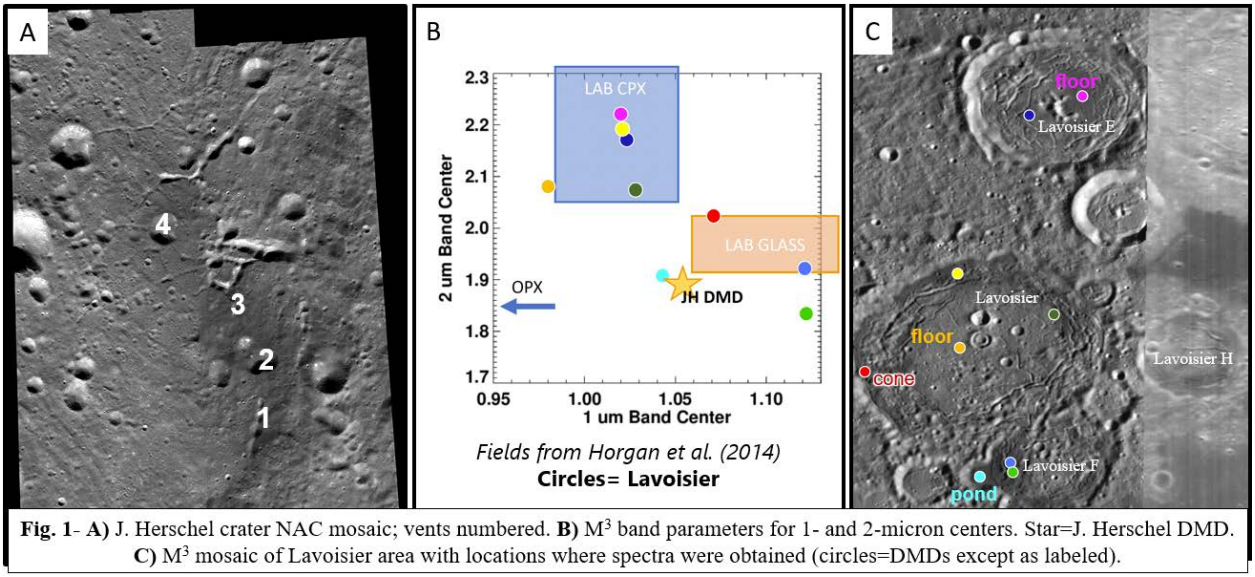

Fig. 1- **A)** J. Herschel crater NAC mosaic; vents numbered. **B)** M^3 band parameters for 1- and 2-micron centers. Star=J. Herschel DMD. **C)** M^3 mosaic of Lavoisier area with locations where spectra were obtained (circles=DMDs except as labeled).

low (~0.05 wt%) [24], suggesting a possible green glass composition [e.g., 1]. Our M^3 analyses near vents 1 and 2 (**Fig. 1**) suggest a composition that is rich in pyroclastic glass, and possibly hosting olivine, but is mixed with orthopyroxene-dominant crater floor deposits, consistent with earlier results [1].

Lavoisier: Previously, 18 potential vents were identified within floor-fractured Lavoisier crater as well as Lavoisier F, H, and E craters [see map in 6]. The distribution of the vents and low-albedo deposits correlate well with the observed fracture structures, including candidate pyroclastic, spatter, and mare basalt effusions [6,25]. Each crater hosts at least one potential pyroclastic deposit, but the craters have varying apparent TiO_2 signatures ranging from none to ~6 wt%. Lavoisier H and F craters (diameters ~31 and 45 km) have domed floors, with deposits concentrated at lower elevations around the edges. Lavoisier E and Lavoisier craters (diameters ~48 and 70 km) have flat and concave floor profiles, respectively, with candidate DMDs mostly along concentric fracture systems, but with the more confidently identified pyroclastics located around the edges of the floor.

Compositions: Our M^3 analysis of the Lavoisier area deposits indicates spectral diversity (**Fig. 1**). Areas within Lavoisier crater and Lavoisier E, particularly their floors, are spectrally clinopyroxene-dominant with lesser absorptions from orthopyroxene, indicating they are mafic but not glass-rich. Several low-albedo areas, including a possible spatter cone, a ponded deposit, and a DMD are spectrally dominated by Fe-bearing glass. Notably, the DMD within Lavoisier F is estimated to be >80 wt% Fe-bearing glass mixed with orthopyroxene from the crater floor.

Summary: The pyroclastic eruptions in J. Herschel crater likely resulted from floor-fractured crater volcanic activity [26,27], where magma intruded beneath a pre-existing impact crater and pressures were sufficient to propagate gas and magma to the surface. Eruptions became focused at the vent locations. In the south, the deposit is ~20 km in width, with an elongated vent (#2) that is ~8 km in maximum width (**Fig. 1**). The V-shaped vent interior and an interior elevation below that of the surrounding terrain suggest predominantly explosive eruptions [3]. The observed distribution of juvenile materials is typical of relatively cool, short-duration, localized eruptions [e.g., 1] where juvenile materials are concentrated near the vent.

The eruptions in the four Lavoisier craters likely also resulted from volcanism associated with magmatic intrusions into, and uplift of, the crater floor structures [6]. The mineralogic and compositional diversity in this region suggests separate magmatic events for the deposits within the closely spaced craters. Compositional and morphology diversity of deposits within each crater likely stems from variations in eruption conditions, including their influences on the thickness and dispersion of emplaced pyroclastics near vents as well as the mode of magmatic intrusion and uplift [27-29].

Conclusions: Our analyses fit into the evolving model that small lunar pyroclastic deposits have a complex history and come in several flavors along a continuous spectrum: 1) glass-dominated, highly explosive, and volatile-rich eruptions; 2) glass-rich, with a significant country rock component, explosive eruptions with moderate amounts of erupted pyroclastics; and 3) pyroclastics with glass and crystalline components. Other types of crystalline or fragmental pyroclastics may also exist on the Moon but are not easily discerned with existing datasets. J. Herschel and many deposits around Lavoisier crater fit into category 2, mostly a mixture of glass and country rock, whereas Lavoisier F DMD and pond and Lavoisier cone fit into category 3. The range of morphologies for those lower albedo deposits suggests that their glass component formed from mildly to moderately explosive eruptions during eruption of intruded magma beneath the crater floor.

Acknowledgments: Data from NASA's Planetary Data System (PDS) and JAXA's archive. This work supported by a NASA LDAP Grant. K.I. by the LPI Summer Intern Program in Planetary Science and the LPI CA. J.S., K.B., and T.G. partly supported by LRO.

References: [1] Jawin et al. (2015) JGR-P 10.1002/ 2014JE004759. [2] Gaddis et al. (2000) JGR 105: 4245-4262. [3] Hawke et al. (1989) Proc. LPSC: 255-268. [4] McCord et al. (1981) JGR 86: 10883-10892. [5] Hawke and Head (1980) LPSC, pp 416-417. [6] Ivey et al. (2022) LPSC abs 1213. [7] Souchon et al. (2013) Icarus 225: 1-14. [8] Delano 1986 Proc. LPSC, D201-D213. [9] Lawrence & Hawke (2008) LPSC abs 1804. [10] van der Bogert et al. (2021) Planet. Sci. J. 10.3847/PSJ/abedbb. [11] Robinson et al. (2010) Space Sci. Rev. 150: 81-124. [12] Boyd et al. (2012) LPSC abs 2795. [13] Haruyama et al. (2012) LPSC abs 1200. [14] Barker et al. (2016) Icarus 273:346-355. [15] Ohtake et al. (2008) Earth, Planets, Space 60: 257-264. [16] Otake et al. (2012) LPSC abs 1905. [17] Pieters et al. (2009) Current Sci. 96: 500-505. [18] Eliason et al. (1999) LPSC abs 1933. [19] Lemelin et al. (2015) JGR-P 10.1002/ 2014JE004778. [20] Bennett et al. (2016) Icarus 273: 296-314. [21] Horgan et al. (2014) Icarus 234: 132-154. [22] Trang et al. (2017) Icarus 283: 232-253. [23] Stopar et al. (2019) LPSC abs 1937. [24] Lucey et al. (2000) JGR-P 105: 20297-20305. [25] Gustafson et al. (2012) LPSC, abs 9036. [26] Head and Wilson (2017) Icarus 283: 176-223. [27] Jozwiak et al. (2015) Icarus 248: 424-447. [28] Morgan et al. (2021) J. Volc. Geotherm. Res. 10.1016/j.volgeores.2021.107217. [29] Keske et al. (2020) EPSL 10.1016/j.epsl/2020.116426.